

# Optical properties of graphene

L.A. Falkovsky<sup>1,2</sup>

<sup>1</sup>*L.D. Landau Institute for Theoretical Physics, Moscow 117334, Russia*

<sup>2</sup>*Institute of the High Pressure Physics, Troitsk 142190, Russia*

Reflectance and transmittance of graphene in the optical region are analyzed as a function of frequency, temperature, and carrier density. We show that the optical graphene properties are determined by the direct interband electron transitions. The real part of the dynamic conductivity in doped graphene at low temperatures takes the universal constant value, whereas the imaginary part is logarithmically divergent at the threshold of interband transitions.

PACS numbers:

## I. INTRODUCTION

Monolayer and bilayer graphenes are gapless two-dimensional (2D) semiconductors whereas its 3D predecessor, graphite, is a semimetal. Hence the dimensional effects can be studied for the unique substance. Monolayer graphene has a very simple electron band structure. Near the energy  $\varepsilon = 0$ , the energy bands are cones  $\varepsilon_{1,2}(\mathbf{p}) = \pm vp$  at the  $K$  points in the 2D Brillouin zone with the constant velocity parameter  $v = 10^8$  cm/s. Such a degeneration is conditioned by symmetry because the small group  $C_{3v}$  of the  $K$  points has a two-dimensional representation.

While the carrier concentration is decreasing in the field gate experiment, the graphene conductivity at low temperatures goes to the finite minimal values. Much theoretical efforts have been devoted to evaluate the minimal conductivity in different approaches. Theoretical and experimental researches show that the main mechanism of the carrier relaxation is provided by the charged impurities and gives the collision rate  $\tau^{-1} \sim 2\pi^2 e^4 n_{imp} / \hbar \epsilon_g^2 \varepsilon$ , where  $\epsilon_g$  is the dielectric constant of graphene,  $\varepsilon$  is the characteristic electron energy (of the order of the Fermi energy or temperature), and  $n_{imp}$  is the density of charged impurities per the unit surface. The general quantum expression for the conductivity depending on the frequency  $\omega$  and wave vector  $k$  has been derived in our paper<sup>1</sup>. In various limiting cases, our result coincides with the formulas of Refs.<sup>2,3</sup>. This expression is valid under a restriction that the collision rate of carriers is less than the frequency and spatial dispersion,  $\tau^{-1} \ll \omega, kv$ . In the optical range, we can neglect the spatial dispersion of conductivity compared with the frequency dependence and use the dynamical conductivity  $\sigma(\omega)$  to study the graphene optical properties<sup>4</sup>. The optical visibility of both monolayer and bilayer graphene was theoretically studied in Ref.<sup>5</sup> focusing on the role of the underlying substrate. Recently, graphene transmittance spectra were observed<sup>6</sup> and the dynamical conductivity was found as  $\sigma(\omega) = e^2/4\hbar$  in agreement with the theory<sup>1,2,3</sup>.

In the present paper, we analyze in detail the optical properties of the graphene monolayer and multilayers. We use the dynamic conductivity  $\sigma$  as a function of fre-

quency  $\omega$ , temperature  $T$ , and chemical potential  $\mu$ . The chemical potential of ideal pure graphene at any temperature is at the crossing of the bands  $\varepsilon_{1,2}$ . With the help of the gate voltage, one can control the density and type ( $n$  or  $p$ ) of carriers varying their chemical potential. Using the dynamic conductivity and the appropriate boundary conditions at interfaces, we calculate the reflection and transmission coefficients of graphene monolayer and multilayers with varying carrier concentration.

## II. OPTICAL CONDUCTIVITY OF GRAPHENE

The general expression for the conductivity used here is obtained in the previous paper<sup>1</sup>. For high frequencies,  $\omega \gg (kv, \tau^{-1})$ , the dynamical conductivity [see Eq. (8) in Ref.<sup>1</sup>] is given by

$$\sigma(\omega) = \frac{e^2 \omega}{i\pi \hbar} \left[ \int_{-\infty}^{+\infty} d\varepsilon \frac{|\varepsilon|}{\omega^2} \frac{df_0(\varepsilon)}{d\varepsilon} - \int_0^{+\infty} d\varepsilon \frac{f_0(-\varepsilon) - f_0(\varepsilon)}{(\omega + i\delta)^2 - 4\varepsilon^2} \right], \quad (1)$$

where  $f_0(\varepsilon) = \{\exp[(\varepsilon - \mu)/T] + 1\}^{-1}$  is the Fermi function.

The first term in Eq. (1) corresponds to the intraband electron-photon scattering processes. Integrating, we obtain explicitly:

$$\sigma^{intra}(\omega) = \frac{2ie^2 T}{\pi \hbar (\omega + i\tau^{-1})} \ln [2 \cosh(\mu/2T)]. \quad (2)$$

Here, we write  $\omega + i\tau^{-1}$  instead of  $\omega$  in order to take into account the electron-impurity scattering processes. In such a form the intraband conductivity coincides with the Boltzmann-Drude expression. For the Fermi-Dirac statistics,  $\mu \gg T$ , the intraband conductivity takes the form

$$\sigma^{intra}(\omega) = \frac{ie^2 |\mu|}{\pi \hbar (\omega + i\tau^{-1})}, \quad (3)$$

where the chemical potential determines the carrier concentration  $n_0 = (\mu/\hbar v)^2/\pi$ .

The second term in Eq. (1), where  $\delta \rightarrow 0$  is infinitesimal quantity determining the bypass around the inte-

grand pole, owes its origin to the direct interband electron transitions. The integral is easily evaluated in the case of zero temperature:

$$\sigma^{inter}(\omega) = \frac{e^2}{4\hbar} \left[ \theta(\omega - 2\mu) - \frac{i}{2\pi} \ln \frac{(\omega + 2\mu)^2}{(\omega - 2\mu)^2} \right]. \quad (4)$$

Here and below, we consider for simplicity the case of the positive  $\mu$ . The step function  $\theta(\omega - 2\mu)$  conveys the condition for the interband electron absorption at low temperatures. The expression shows that the interband contribution plays the leading role around the absorption threshold  $\omega \approx 2\mu$  comparatively with the Boltzmann-Drude intraband term, Eqs. (2) and (3), which is important at relatively low frequencies,  $\omega < \mu$ . The logarithmic singularity is cut off with temperature. At the finite, but low temperatures, the following substitutions should be made in Eq. (4)

$$\begin{aligned} \theta(\omega - 2\mu) &\rightarrow \frac{1}{2} + \frac{1}{\pi} \arctan[(\omega - 2\mu)/2T] \\ (\omega - 2\mu)^2 &\rightarrow (\omega - 2\mu)^2 + (2T)^2. \end{aligned} \quad (5)$$

The electron relaxation processes produce similar smearing.

It is useful for numerical calculations to present the difference of the Fermi functions in the second integrand (1) as

$$G(\varepsilon) = \frac{\sinh(\varepsilon/T)}{\cosh(\mu/T) + \cosh(\varepsilon/T)}.$$

Adding and subtracting  $G(\omega/2)$  in the numerator of the integrand, and noticing that the the principal value of the integral with  $G(\omega/2)$  equals to zero, we arrive at the integral without singularities. Then we can write the interband conductivity in the form available for numerical calculations:

$$\sigma^{inter}(\omega) = \frac{e^2}{4\hbar} \left[ G(\omega/2) - \frac{4\omega}{i\pi} \int_0^{+\infty} d\varepsilon \frac{G(\varepsilon) - G(\omega/2)}{\omega^2 - 4\varepsilon^2} \right]. \quad (6)$$

For the Fermi-Dirac and Boltzmann carrier statistics, correspondingly, the first term is given asymptotically by

$$G(\omega/2) = \begin{cases} \theta(\omega - 2\mu), & \mu \gg T, \\ \tanh(\omega/4T), & \mu \ll T. \end{cases} \quad (7)$$

The conductivity calculated with the help of Eqs. (2), (6) is shown in Fig. 1. The step function behavior of the real part (absorption) and logarithmic singularity of the imaginary part are clearly seen at low temperatures. While increasing the temperature, the transition from the Boltzmann statistics to the Fermi-Dirac statistics is also evident.

By using the gate voltage, one can control the density of electrons ( $n_0$ ) or holes ( $-n_0$ ). Then the chemical

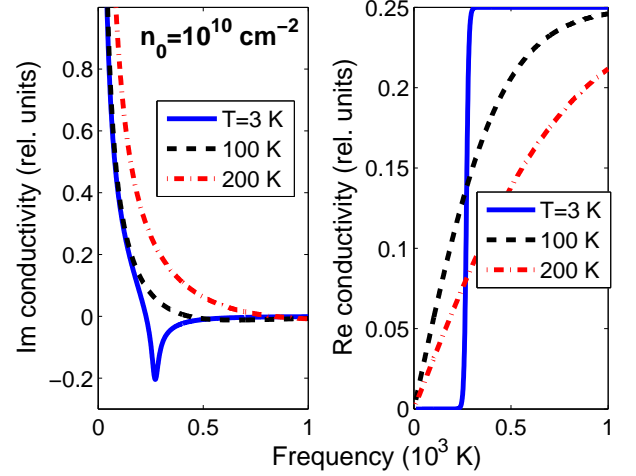


FIG. 1: (color online). Imaginary (left) and real (right) parts of conductivity in units of  $e^2/\hbar$  for graphene doped with the carrier density  $n_0 = 10^{10} \text{ cm}^{-2}$  at temperatures noted at lines. The chemical potential equals to 135, 65, and 33 K at 3, 100, and 200 K, correspondingly.

potential is determined by the condition

$$n_0 = \frac{2}{\pi(\hbar v)^2} \int_0^{+\infty} \varepsilon [f_0(\varepsilon - \mu) - f_0(\varepsilon + \mu)] d\varepsilon. \quad (8)$$

From this expression and Fig. 2(a), one can see that the chemical potential goes to zero while the temperature increases.

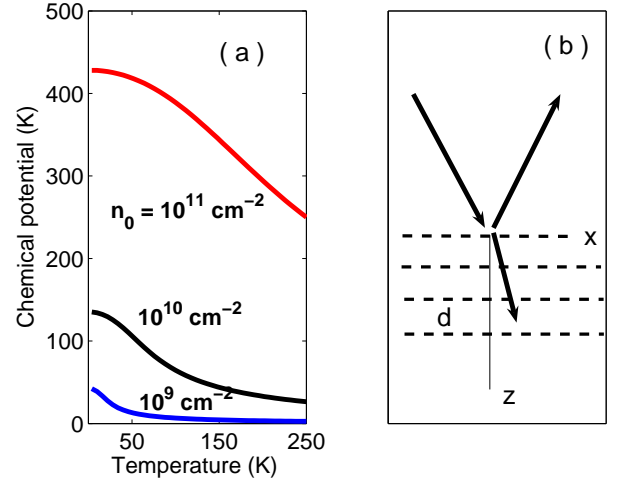


FIG. 2: (color online). (a) Chemical potential (in K) as a function of temperature at carrier densities noted at curves. (b) Multilayers sample and geometry of wave scattering.

### III. SPECTROSCOPY OF GRAPHENE LAYERS

In order to calculate the graphene reflectance, we apply Maxwell's equations

$$\nabla(\nabla \cdot \mathbf{E}) - \nabla^2 \mathbf{E} = \epsilon_0 \frac{\omega^2}{c^2} \mathbf{E} + \frac{4\pi i \omega}{c^2} \mathbf{j}, \quad (9)$$

where  $\epsilon_0$  is the ion contribution into the dielectric constant and  $\mathbf{j}$  is the conductivity current. We consider the case of the  $p$ -polarization, when the field  $\mathbf{E}$  lies in the  $xz$  plane and the current  $\mathbf{j}$  has only the in-layer  $x$  component (see Fig 2b).

#### A. Optics of a monolayer.

Consider the graphene monolayer at  $z = 0$  with  $\epsilon_0 = \epsilon_g$  deposited on the substrate ( $z > 0$ ) with the dielectric constant  $\epsilon_0 = \epsilon_s$  (for graphene suspended in the vacuum,  $\epsilon_s = 1$ ). The ac field is given by the sum of incident and reflected waves in the vacuum,  $z < 0$ , and by the transmitted wave in the substrate. In the geometry considered, the current in graphene monolayer can be written in the form

$$j_x = \sigma(\omega) \delta(z) E_x. \quad (10)$$

Making use of the Fourier transformations with respect to the  $x$  coordinate,  $\mathbf{E} \propto e^{ik_x x}$ , we rewrite the Maxwell equations (9) as follows

$$\begin{aligned} ik_x \frac{dE_z}{dz} - \frac{d^2 E_x}{dz^2} - \epsilon_0 \frac{\omega^2}{c^2} E_x &= \frac{4\pi i \omega}{c^2} j_x, \\ ik_x \frac{dE_x}{dz} + (k_x^2 - \epsilon_0 \frac{\omega^2}{c^2}) E_z &= 0. \end{aligned} \quad (11)$$

The boundary conditions for these equations at  $z = 0$  are the continuity of the field component  $E_x$  and the jump of the electric-induction  $z$  component at the sides of the monolayer:

$$\epsilon_s E_z|_{z=+0} - E_z|_{z=-0} = 4\pi \int_{-0}^{+0} \rho(\omega, k_x, z) dz. \quad (12)$$

The carrier density is connected to the current in Eq. (10) according to the continuity equation

$$\rho(\omega, k_x, z) = j_x(\omega, k_x, z) k_x / \omega.$$

Substituting  $E_z$  from the second Eq. (11) into (12), we find the second boundary condition

$$\frac{\epsilon_s}{k_s^2} \frac{dE_x}{dz} \Big|_{z=+0} - \frac{1}{(k_x^i)^2} \frac{dE_x}{dz} \Big|_{z=-0} = \frac{4\pi\sigma(\omega)}{i\omega} E_x \Big|_{z=0}, \quad (13)$$

where

$$k_s = \sqrt{\epsilon_s(\omega/c)^2 - k_x^2}, \quad k_x^i = \sqrt{(\omega/c)^2 - k_x^2}.$$

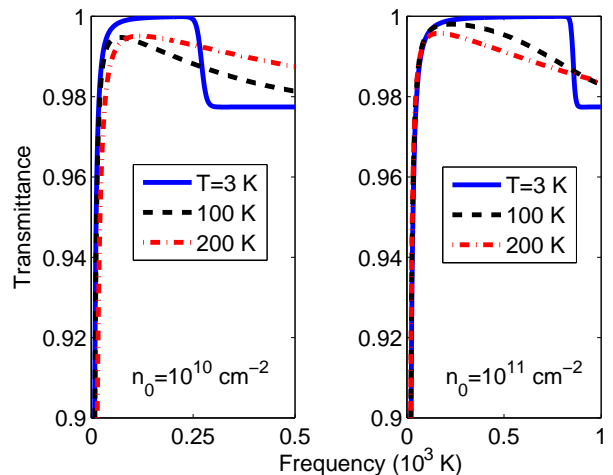


FIG. 3: (color online). Transmittance spectrum of graphene with carrier densities  $n_0 = 10^{10} \text{ cm}^{-2}$  (left) and  $n_0 = 10^{11} \text{ cm}^{-2}$  (right) versus the frequency at temperatures noted at the curves; normal incidence. For the carrier density  $n_0 = 10^{11} \text{ cm}^{-2}$ , the chemical potential equals to 428, 389, and 294 K at 3, 100, and 200 K, correspondingly.

Using the boundary conditions, we find the reflection ( $r$ ) and transmission ( $t$ ) amplitudes

$$r = \frac{1-C}{1+C}, \quad t = \frac{2}{1+C}, \quad (14)$$

where  $C = k_x^i [(4\pi\sigma(\omega)/\omega) + (\epsilon_s/k_s)]$ . The very simple results can be written for graphene suspended in the vacuum, when  $\epsilon_s = 1$  and  $k_s = k_x^i$ . Then, the coefficient  $C$  is close to unity,

$$C = 1 + 4\pi\sigma(\omega) \cos \theta / c, \quad (15)$$

where  $\theta$  is the incidence angle. Therefore, Eqs. (14) yield for the reflected and transmitted amplitudes

$$r = -2\pi\sigma(\omega) \cos \theta / c, \quad t = 1 - 2\pi\sigma(\omega) \cos \theta / c, \quad (16)$$

The transmission coefficient  $|t|^2$  calculated with the help of Eqs. (2), (6), and (14) for normal incidence is shown in Figs. 3 as a function of frequency, temperature, and carrier density. One can see that the deviation of the graphene transmittance from unity is proportional to the dimensionless parameter  $e^2 \max(T, \mu) / \hbar c \omega$ , i.e., it is relatively large at the very low frequencies  $\omega \approx e^2 \max(T, \mu) / \hbar c$ , when the intraband conductivity plays the leading role. At higher frequencies, the interband transitions play the leading role. Then, the transmittance does not depend on frequency, being controlled by the fine structure constant  $e^2 / \hbar c$ . For instance, at normal incidence and  $T \ll \mu < \omega/2$ , the transmission coefficient is given by

$$|t|^2 = 1 - \frac{4\pi}{c} \text{Re} \sigma(\omega) = 1 - \pi \frac{e^2}{\hbar c}, \quad (17)$$

where the logarithmic terms is omitted since it contains the fine structure constant squared. As was found recently<sup>6</sup>, the linear (in the fine structure constant) effect can be observed in graphene at the visible frequencies.

Reflectance increases with the temperature, because the carrier density increases. As the chemical potential decreases with the temperature, the temperature dependence of reflectance is not monotonic as seen clearly in Fig. 3.

### B. Spectroscopy of graphene multilayers.

Let the multilayers cross the  $z$  axis at points  $z_n = nd$ , where  $d$  is the distance between the layers (see Fig. 2b). Such a system can be considered as a model of graphite since the distance  $d = 3.35\text{\AA}$  in graphite is larger than the interatomic distance in the layer. So, we describe the carrier interaction in the presence of ac electric field with the help of self-consistent Maxwell's equations (9). For the  $x$  component of the field  $E_x$ , they give

$$\left( \frac{d^2}{dz^2} + k_s^2 + 2k_s \mathcal{D} \sum_n \delta(z - nd) \right) E_x = 0, \quad (18)$$

where  $\mathcal{D} = 2i\pi\sigma(\omega)k_s/\epsilon_g\omega$ .

For the infinite number of layers in the stack, the solutions of Eq. (18) represent two Bloch states

$$e_{1,2}(z) = e^{\pm ik_z nd} \{ \sin k_s(z - nd) - e^{\mp ik_z d} \times \sin k_s[z - (n+1)d] \}, \quad nd < z < (n+1)d \quad (19)$$

with the quasi-momentum  $k_z$  determined from the dispersion equation

$$\cos k_z d = \cos k_s d - \mathcal{D} \sin k_s d. \quad (20)$$

The dispersion equation describes the electric field excitations in the system. The quasi-momentum  $k_z$  can be restricted to the Brillouin half-zone  $0 < k_z < \pi/d$ , if the parameter  $\mathcal{D}$  is real. In the general case, while taking the interband absorption into account, we fix the choice of the eigen-functions in Eq. (19) by the condition  $\text{Im } k_z > 0$  so that the solution  $e_1$  decreases in the positive direction  $z$ .

In the long-wave limit,  $k_z, k_s \ll 1/d$ , the dispersion equation (20) can be simplified. In this case, the dielectric permittivity can be introduced not only in the normal  $z$  direction,  $\epsilon_{zz} = \epsilon_g \simeq 2.5$ , but in the tangential direction as well, namely,

$$\epsilon_{xx} = \epsilon_g + 4\pi i\sigma(\omega)/\omega d, \quad (21)$$

where  $\sigma(\omega)$  is the dynamic conductivity, Eq. (1), of the one layer. Then the dispersion equation (20) takes the form

$$k_x^2 \epsilon_{xx} + k_z^2 \epsilon_{zz} = (\omega/c)^2 \epsilon_{xx} \epsilon_{zz}. \quad (22)$$

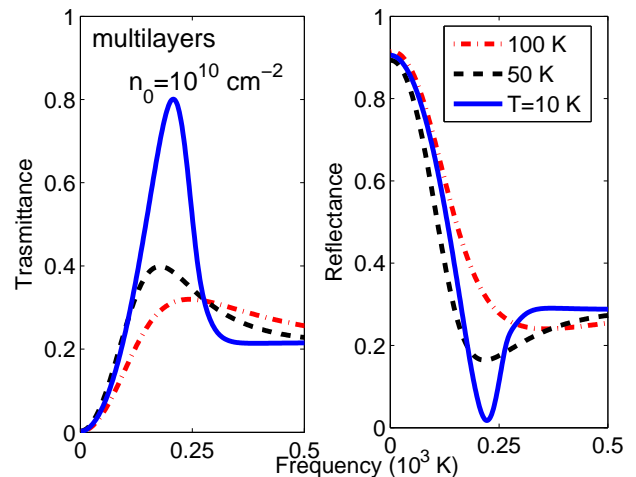


FIG. 4: (color online). Transmittance and reflectance at the normal incidence for a plate with the graphene multilayers and the carrier density  $n_0 = 10^{10} \text{ cm}^{-2}$  in a layer; the distance between layers  $d = 3.35\text{\AA}$ , thickness of the plate is  $l = 100d$ , temperatures are noted at curves.

We see from this equation, that the weakly damped solutions (for normal incidence,  $k_x = 0$ ) exist, if the real part of the dielectric function  $\epsilon_{xx}$  is positive and larger than the imaginary part. According Eqs. (3) and (4), this condition is fulfilled just below the threshold of interband transitions. Due to these weakly damped waves, the maximum in transmittance and the corresponding minimum in reflectance of the multilayer system appear at temperatures below the threshold as shown in Fig. 4.

Calculations done for a thin plate with the stack of graphene multilayers give the following result for the transmission amplitude

$$t = \frac{4k_z k_z^i}{(k_z + k_z^i)^2 f - (k_z - k_z^i)^2 f^{-1}}, \quad (23)$$

where  $f = \exp(-ik_z l)$ ,  $k_z^i = (\omega/c) \cos \theta$ ,  $k_z$  is determined by the dispersion equation (22) at fixed values of  $\omega$  and  $k_x$ .

At higher frequencies,  $\omega > 2\mu = 270 \text{ K}$  (in Fig. 4), after the downfall, the reflection coefficient corresponds with the interband absorption presented by the  $\theta$ -singularity in the real part of conductivity. In contrast to the monolayer, the effect of carriers in the multilayers is controlled by the large dimensionless factor  $(e^2/\hbar\epsilon_g\omega d)$  [see Eq. (21)] of the function varying rapidly at  $\omega \approx 2\mu$ . It means that the interband absorption can be observed at relatively large frequencies and low temperatures. Notice that observations of the absorption threshold provide a direct method of carrier density characterization in graphene.

#### IV. CONCLUSION

In conclusion, we have developed the detailed microscopic theory of the graphene monolayer and multilayers spectroscopy. We have shown that the reflectance from the monolayer is determined for infra-red region by the intraband Drude-Boltzmann conductivity and for higher frequencies by the interband absorption. We have argued that at low temperatures and high carrier densities, the

reflectance from multilayers has the sharp downfall with the subsequent plateau. These features are caused by excitations of propagating waves and the direct interband electron transitions.

#### Acknowledgments

This work is supported by the Russian Foundation for Basic Research (grant No. 07-02-00571).

---

<sup>1</sup> L.A. Falkovsky and A.A. Varlamov, cond-mat/0606800, Eur. Phys. J. B **56**, 281 (2007).

<sup>2</sup> V.P. Gusynin, S.G. Sharapov, and J.P. Carbotte, Phys. Rev. **B 75**, 165407 (2007); cond-mat/0607727, Phys. Rev. Lett. **96**, 256802 (2006).

<sup>3</sup> J. Cserti, Phys. Rev. **B 75**, 033405 (2007).

<sup>4</sup> L.A. Falkovsky and S.S. Pershoguba, Phys. Rev. **B 76**,

153410 (2007).

<sup>5</sup> D.S.L. Abergel, A. Russell, and V. I. Fal'ko, cond-mat/0705.0091, unpublished.

<sup>6</sup> R.R. Nair, P. Blake, A.N. Grigorenko, K.S. Novoselov, T.J. Blooth, T. Stauber, N.M.R. Peres, and A.K. Geim, cond-mat/0803.3718, unpublished.